A note on the effective slip properties for microchannel flows with ultrahydrophobic surfaces

M. Sbragaglia
Faculty of Applied Sciences, IMPACT, and Burgerscentrum, University of Twente, AE 7500 Enschede, The Netherlands

A. Prosperetti
Faculty of Applied Sciences, IMPACT, and Burgerscentrum, University of Twente, AE 7500 Enschede, The Netherlands and Department of Mechanical Engineering, The Johns Hopkins University, Baltimore, Maryland 21218

(Received 2 November 2006; accepted 21 February 2007; published online 23 April 2007)

A type of superhydrophobic surface consists of a solid plane boundary with an array of grooves which, due to the effect of surface tension, prevent a complete wetting of the wall. The effect is greatest when the grooves are aligned with the flow. The pressure difference between the liquid and the gas in the grooves causes a curvature of the liquid surface resisted by surface tension. The effects of this surface deformation are studied in this paper. The corrections to the effective slip length produced by the curvature are analyzed theoretically and a comparison with available data and related mathematical models is presented. © *2007 American Institute of Physics*.
[DOI: 10.1063/1.2716438]

I. INTRODUCTION

Large pressure drops are necessary to cause liquid flow in micro- and nano-channels. The small values of naturally occurring slip lengths on hydrophobically coated surfaces, typically of the order of some nanometers,[1–3] are in most cases insufficient to significantly affect the required pressure gradients, as also confirmed by some theoretical analyses.[4–6] With the recent increasing interest in such systems,[7,8] efforts to reduce these large pressures have been made. One promising avenue is the so-called superhydrophobic surfaces,[9–14] in which the wall stress is decreased by reducing the liquid-solid contact area.[1,8] The idea is to cover the surface of interest with structures such as posts, grooves, or others, over which the liquid surface remains suspended due to the effect of surface tension. The effect is equivalent to the introduction of an effective slip length of a magnitude comparable with the size of the geometrical features on the surface. This arrangement has been studied by several authors both experimentally[9–11,15] and theoretically.[4–6,16–21] In particular, Lauga and Stone[17] studied the flow in a circular tube, the wall of which consisted of a periodic sequence of free-slip and no-slip annuli and quantified the effect of the boundary heterogeneity on the slip length. The authors in Ref. 5 considered a more general situation in which the heterogeneous flat boundary was endowed with a spatially varying slip length. Ou and co-workers[9,10] investigated the performance of a microchannel with a rectangular cross section, the floor of which contained a series of gas-filled grooves aligned with the flow. This configuration resembles the situation studied theoretically by Philip,[18] who modeled several situations with mixed slip/no-slip plane boundaries. In a system of the type studied by Ou and co-workers, the liquid surface becomes convex toward the gas occupying the groove due to the high pressure in the channel, with the radius of curvature determined by the balance of the pressure difference and surface tension. The importance of this effect increases with increasing pressure and may be expected to become significant as the channel size decreases and the pressure levels correspondingly increase. The purpose of the present paper is to calculate the correction to the effective slip length due to these capillary effects. While the correction is small for the case considered by Ou and co-workers, one can easily envisage practical cases in which the effect would be important. Our approach is perturbative and rests on the smallness of the deformation of the free surface.

II. CURVATURE EFFECTS ON A PERIODIC FREE SHEAR PATTERN: FORMULATION OF THE PROBLEM

We consider a liquid flowing in a rectangular channel, the floor of which contains equally spaced slots aligned with the flow (see Fig. 1, top). Surface tension prevents the liquid from filling the slots, but the pressure in the channel causes the liquid free surface to bow into them. We assume that this curvature is sufficiently small that the advancing contact angle is not exceeded, so that the contact line remains pinned at the edge of the grooves (see Fig. 1, bottom).

If there is a sufficient number of slots, we can consider the flow as consisting of the periodic repetition of equal cells similar to the one shown in Fig. 1. In this figure, the top boundary, at a distance L^* above the floor, is the roof of the channel, the dashed vertical lines are periodicity boundaries, and the lower boundary of the liquid region consists of a free-slip portion along a free surface S, occupying the range $|x^*|<c^*$, and no-slip portions on either side of it, for $c^*<|x^*|<H^*/2$, where H^* is the dimensional cell width. Lengths will be rendered dimensionless with respect to $H^*/2\pi$, so that $0\leqslant c<\pi$ and $L=2\pi L^*/H^*$. It will also be convenient to introduce a slip fraction defined as

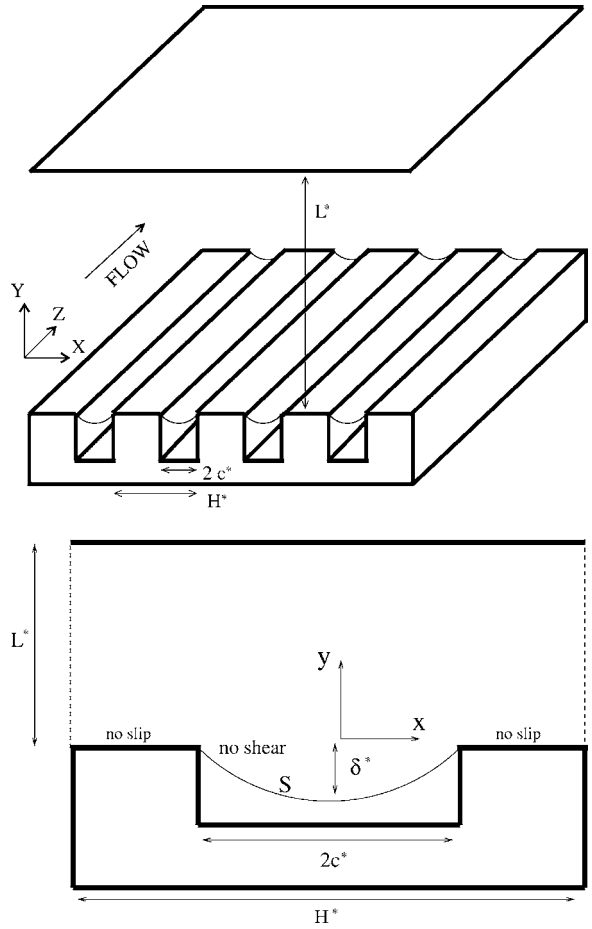

FIG. 1. Schematic geometry of the problem studied in this paper. The floor of a channel with height L^* contains a series of regularly spaced grooves parallel to the flow direction (top). When the number of grooves is large, the situation can be approximated by the periodic repetition of a fundamental cell of width H^* such as the one shown here (bottom). The width of the groove, where the shear stress is essentially zero, is $2c^*$. For small deformation, the maximum penetration of the free surface S into the groove is $\delta^* = (c^*)^2/2R^*$, where R^* is the radius of curvature of the free surface.

$$\xi = \frac{2c^*}{H^*} = \frac{c}{\pi}. \tag{1}$$

In fully developed conditions, only the axial velocity component w^* is nonzero. Upon nondimensionalizing it with respect to the axial pressure gradient $|dp^*/dz^*|$ and liquid viscosity μ, $w = (2\pi/H^*)^2 \mu w^*/(-dp^*/dz^*)$, this quantity satisfies

$$\partial_{xx} w + \partial_{yy} w = -1, \tag{2}$$

where we have assumed the pressure field to be uniform over the cross section. The field w satisfies the no-slip condition on the roof of the cell and periodicity conditions on its lateral boundaries,

$$w(x,L) = 0, \quad \partial_x w(\pm\pi, y) = 0. \tag{3}$$

On the floor of the cell, the no-slip condition applies away from the groove,

$$w(x,0) = 0 \quad \text{for } c < |x| < \pi, \tag{4}$$

while there is no tangential stress on the free surface S,

$$\boldsymbol{n} \cdot \nabla w = 0 \quad \text{on } S, \tag{5}$$

where $\boldsymbol{n}$ is the normal to the free surface. From a knowledge of w, one can calculate the flow rate in the channel

$$Q = \int_A w(x,y)\, dA, \tag{6}$$

where A is the total cross-sectional area bounded by the solid walls and the free surface.

One can define an effective slip length λ by equating the actual flow rate Q with the flow rate Q_{eff} that would be found in a rectangular channel of height L and width 2π with a partial-slip condition applied at the bottom wall,

$$w_{\text{eff}}(x,0) = \lambda \partial_y w_{\text{eff}}(x,0). \tag{7}$$

The flow rate in this latter case is readily calculated,

$$Q_{\text{eff}} = \frac{\pi L^3}{6}\left(1 + 3\frac{\lambda}{L}\right). \tag{8}$$

III. PERTURBATION PROBLEM

With the small dimensions of practical interest, the curvature of the free surface is small and we represent it in the form

$$y + \epsilon \eta(x) = 0, \tag{9}$$

in which the parameter ϵ, to be estimated presently, is taken to be small compared to 1. With this approximation it is easy to show that, correct to first order in ϵ, the free-shear condition (5) is

$$\tau_{yz} + \epsilon \frac{d\eta}{dx} \tau_{xz} = 0, \tag{10}$$

where $\tau_{iz} = \partial_i w$, $i = x, y$, denotes the only nonvanishing components of the viscous stress. The smallness of ϵ suggests a perturbation approach to the solution of the problem and we write

$$w = w^{(0)} + \epsilon w^{(1)} + o(\epsilon). \tag{11}$$

The field $w^{(0)}$ satisfies (2) while $w^{(1)}$ is harmonic. Both satisfy the conditions (3) and (4) on the solid and periodicity boundaries while, by a Taylor-series expansion in ϵ, we find the boundary conditions in the groove as

$$\partial_y w^{(0)}(x,0) = 0 \quad \text{for } |x| < c \tag{12}$$

and

$$\partial_y w^{(1)}(x,0) = -\partial_x [\eta(x) \partial_x w^{(0)}(x,0)] - \eta(x) \quad \text{for } |x| < c \tag{13}$$

at orders ϵ^0 and ϵ, respectively. When the expansion (11) is used to calculate the flow rate, we find

$$Q = Q^{(0)} + \epsilon [Q_1^{(1)} + Q_2^{(1)}] + o(\epsilon) \tag{14}$$

with

$$Q^{(0)} = \int_{-\pi}^{\pi} dx \int_0^L dy w^{(0)}(x,y), \tag{15}$$

$$Q_1^{(1)} = \int_{-\pi}^{\pi} dx \int_0^L dy w^{(1)}(x,y), \tag{16}$$

and

$$Q_2^{(1)} = \int_{-c}^{c} w^{(0)}(x,0)\,\eta(x)dx. \tag{17}$$

This second term of the $\mathcal{O}(\epsilon)$ contribution to the flow rate arises from the deformation of the free surface.

In order to estimate the parameter ϵ and the shape of the deformed free surface, it is convenient to revert temporarily to dimensional quantities. From the pressure in the channel P^*_{ch} and in the gas occupying the slot under the liquid, P^*_{gas}, we can calculate the radius of curvature R^* of the interface from Laplace's formula as

$$R^* = \frac{\sigma}{P^*_{ch} - P^*_{gas}}, \tag{18}$$

where σ is the surface-tension coefficient. If $P^*_{ch} > P^*_{gas}$, the surface bows into the groove, while the curvature is in the opposite direction when $P^*_{ch} < P^*_{gas}$. Thus, in principle, a control of this pressure difference would permit some control on the effective slip length, as we will demonstrate.

The circle of radius R^* passing through the points $x^* = \pm c^*$, $y^* = 0$ has the equation

$$(x^*)^2 + [y^* - \sqrt{(R^*)^2 - (c^*)^2}]^2 = (R^*)^2 \tag{19}$$

from which

$$y^* = \sqrt{(R^*)^2 - (c^*)^2} - \sqrt{(R^*)^2 - (x^*)^2} \simeq -\frac{1}{2R^*}[(c^*)^2 - (x^*)^2]. \tag{20}$$

This relation can be written in the form (9) with

$$\epsilon^* = \frac{1}{2R^*} = \frac{P^*_{ch} - P^*_{gas}}{2\sigma} \tag{21}$$

so that

$$\epsilon = \frac{H^*}{4\pi}\frac{P^*_{ch} - P^*_{gas}}{\sigma}. \tag{22}$$

Upon reverting to dimensionless quantities, the free surface shape η in (9) is thus found to be given by

$$\eta = c^2 - x^2. \tag{23}$$

The pressure in the channel falls in the direction of the flow, which will lead to an axial variation of R. This effect is usually sufficiently slow[9,10] as not to significantly affect the assumption of parallel flow.

The previous estimate assumes that the pressure in the gas remains unperturbed by the curvature of the interface. At a mathematical level, this assumption is justified by the fact that, since the surface curvature if of order ϵ, it is consistent to consider P^*_{gas} with an $O(\epsilon^0)$ accuracy. Physically, the response of P^*_{gas} to the curving interface will depend on the specifics of the experimental setup and dimensions (e.g., the inlet/outlet conditions, the depth of the grooves, and others), which cannot be accounted for without introducing additional parameters. In any event, the behavior of P^*_{gas} can be accounted for by a suitable adjustment of the numerical value of the parameter ϵ, which has no effect on the developments that follow.

IV. ZEROTH-ORDER SOLUTION: LAMINAR FLOW OVER A FLAT PATTERNED SURFACE

Following the approach proposed by Philip,[18] we seek the solution in the form

$$w^{(0,L)}(x,y) = -\frac{1}{2}y(y-L) + \frac{1}{2}L\tilde{w}^{(0,L)}(x,y), \tag{24}$$

where the first term is the standard two-dimensional channel flow profile with no-slip top and bottom walls and $\tilde{w}^{(0,L)}$ is the correction due to the free-slip portion of the lower boundary. Evidently $\tilde{w}^{(0,L)}$ satisfies Laplace's equation with conditions (3) and (4) on the solid and periodicity boundaries, while

$$\partial_y \tilde{w}^{(0,L)}(x,0) = -1 \quad \text{for } |x| < c. \tag{25}$$

Since $\tilde{w}^{(0,L)}$ is periodic in x and even, it can be expanded in a Fourier cosine series in x, after which the requirement that it be harmonic determines the y dependence,

$$\tilde{w}^{(0,L)}(x,y) = \frac{a_0^{(0,L)}}{2}\left(1 - \frac{y}{L}\right) + \sum_{n=1}^{\infty} a_n^{(0,L)}[1 - e^{-2n(L-y)}]e^{-ny}\cos(nx). \tag{26}$$

This form ensures the absence of slip on the channel roof $y=L$; the boundary conditions at the lower wall lead to the dual series equations

$$\frac{a_0^{(0,L)}}{2} + \sum_{n=1}^{\infty} a_n^{(0,L)}(1 - e^{-2nL})\cos(nx) = 0, \quad c < x < \pi, \tag{27}$$

$$\frac{a_0^{(0,L)}}{2L} + \sum_{n=1}^{\infty} a_n^{(0,L)} n(1 + e^{-2nL})\cos(nx) = 1, \quad 0 < x < c. \tag{28}$$

This problem was solved by Philip,[18] but his procedure was different from that adopted here and it is shown in Appendix A that his solution is correctly recovered. The flow rate $Q^{(0)}$ is readily calculated from (24) and (26):

$$Q^{(0)} = \frac{\pi L^3}{6}\left(1 + 3\frac{a_0^{(0,L)}}{2L}\right). \tag{29}$$

For a finite height L, it does not seem possible to solve the dual-series equations (27) and (28) exactly. We have calculated the solution numerically as explained in Appendix C. The case of infinite depth can, however, be treated analytically (Appendix A). In particular, one finds

$$a_0^{(0,\infty)} = -4\log\left(\cos\frac{c}{2}\right) \tag{30}$$

and

$$\tilde{w}^{(0,\infty)}(x,0) = 2\,\mathrm{arccosh}\left(\frac{\cos\frac{x}{2}}{\cos\frac{c}{2}}\right), \quad |x| < c. \tag{31}$$

A quantity that is needed to compute the first-order correction is $\partial_x\tilde{w}^{(0,L)}(x,0)$, as is shown by (13). This quantity can be easily expressed as

$$\partial_x\tilde{w}^{(0,L)}(x,0) = \sum_{n=1}^{\infty} n a_n^{(0,L)} \sin(nx)[e^{-2nL} - 1] \tag{32}$$

and, in the limit $L/H \to \infty$, the series can be summed exactly to obtain (see Appendix A)

$$\partial_x\tilde{w}^{(0,\infty)}(x,0) = -\sqrt{2}\frac{\sin\frac{x}{2}}{\sqrt{\cos x - \cos c}}, \quad |x| < c. \tag{33}$$

V. FIRST-ORDER PROBLEM

We seek the solution for the first-order correction to the velocity field in a form similar to (24), $w^{(1,L)} = \frac{L}{2}\tilde{w}^{(1,L)}$, where

$$\tilde{w}^{(1,L)}(x,y) = \frac{a_0^{(1,L)}}{2}\left(1 - \frac{y}{L}\right) + \sum_{n=1}^{\infty} a_n^{(1,L)}[1 - e^{-2n(L-y)}]e^{-ny}\cos(nx). \tag{34}$$

According to (16), the contribution to the flow rate given by the velocity $w^{(1,L)}$ is

$$Q_1^{(1)} = \frac{\pi}{4}a_0^{(1,L)}L^2. \tag{35}$$

The no-slip condition imposed on (34) is expressed by

$$\frac{a_0^{(1,L)}}{2} + \sum_{n=1}^{\infty} a_n^{(1,L)}(1 - e^{-2nL})\cos(nx) = 0, \quad c < x < \pi \tag{36}$$

while the zero-shear condition (13) becomes

$$\frac{a_0^{(1,L)}}{2L} + \sum_{n=1}^{\infty} a_n^{(1,L)} n(1 + e^{-2nL})\cos(nx) = \partial_x[\eta\partial_x\tilde{w}^{(0,L)}(x,0)] + \frac{2\eta(x)}{L}, \quad 0 < x < c \tag{37}$$

with $\partial_x\tilde{w}^{(0,L)}(x,0)$ given by (32). Again, this dual-series system cannot be solved analytically except in the case of infinite depth for which we find (see Appendix B)

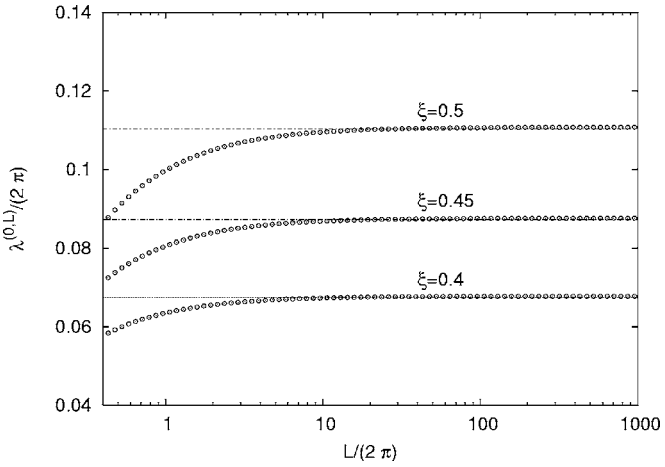

FIG. 2. The zero-order effective slip length $\lambda^{(0,L)}$ normalized by the horizontal period 2π as a function of the channel height L also normalized by 2π for various values of the slip fraction $\xi = c/\pi$; the nomenclature is defined in Fig. 1. The symbols are results obtained by solving numerically (27) and (28). The straight lines are the limit $L/(2\pi) \to \infty$ given by the exact solution (44).

$$a_0^{(1,\infty)} = -\frac{4}{\pi}\int_0^c \frac{\sin^2\frac{x}{2}(c^2 - x^2)dx}{\cos x - \cos c} = -\frac{2}{\pi}\int_0^c \frac{(1 - \cos x)(c^2 - x^2)dx}{\cos x - \cos c}. \tag{38}$$

For general L, we have to resort to a numerical solution.

VI. EFFECTIVE SLIP LENGTH

We expand the slip length similarly to (14) as

$$\lambda^{(L)} = \lambda^{(0,L)} + \epsilon[\lambda_1^{(1,L)} + \lambda_2^{(1,L)}] + o(\epsilon), \tag{39}$$

in which $\lambda^{(0,L)}$ is the contribution of the unperturbed flow (i.e., with a flat free-slip surface), $\lambda_1^{(1,L)}$ is the contribution of the perturbed velocity profile, and $\lambda_2^{(1,L)}$ is the contribution of the unperturbed velocity arising from the deformation of the flow passage. From (8), (14), (29), and (35), we find

$$\lambda^{(0,L)} = \frac{a_0^{(0,L)}}{2}, \tag{40}$$

$$\lambda_1^{(1,L)} = \frac{a_0^{(1,L)}}{2}, \tag{41}$$

$$\lambda_2^{(1,L)} = \frac{2}{\pi L^2}\int_{-c}^{c} w^{(0)}(x,0)(c^2 - x^2)dx. \tag{42}$$

Figure 2 is a graph of the zero-order slip length normalized by the width of the periodic cell,

$$\frac{\lambda^{(0,L)}}{2\pi} = \frac{\lambda^{(0,L^*)}}{H^*}, \tag{43}$$

as a function of the normalized channel height $L/(2\pi) = L^*/H^*$ for various values of the slip fraction ξ. The straight

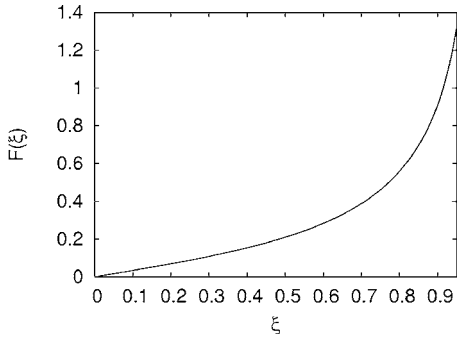

FIG. 3. The function $F(\xi)$ as it is defined in (46) is plotted as a function of the slip percentage ξ.

lines are the corresponding analytical results for $L/(2\pi) \to \infty$ given by (see Appendix A)

$$\frac{\lambda^{(0,\infty)}}{2\pi} = -\frac{1}{\pi}\log\left(\cos\frac{\pi\xi}{2}\right). \tag{44}$$

While convergence to this result is evident from the figure, it is also clear that the rate of convergence becomes slower and slower as the free-slip fraction increases. This feature is a consequence of the fact that, as follows from Eq. (7) and as is explicitly shown by (44), the slip length diverges to infinity when $\xi \to 1$. Figures 4–6 show the first-order corrections, $\lambda_1^{(1,L)}$ and $\lambda_2^{(1,L)}$, found from the numerical solution of (36) and (37), also for various values of the slip fraction ξ. The correction $\lambda_1^{(1,L)}$ (Figs. 4 and 5) approaches a negative value (straight lines of Fig. 4) in the limit of large channel height where, as shown in Appendix B, $\epsilon\lambda_1^{(1,\infty)}$ normalized to the pattern dimension can be represented as

$$\epsilon\frac{\lambda_1^{(1,\infty)}}{2\pi} = -\frac{\delta^*}{H^*}F(\xi), \quad \delta^* = \frac{(c^*)^2}{2R^*} \tag{45}$$

with

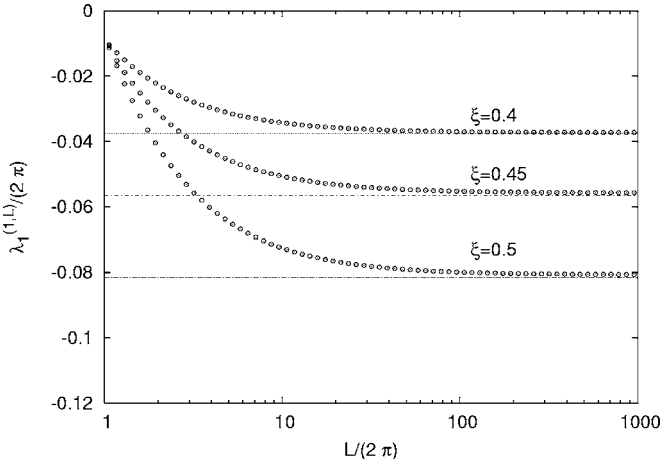

FIG. 4. Results for the quantity $\lambda_1^{(1,L)}/(2\pi)$ as a function of the dimensionless ratio $L/(2\pi)$ for various values of ξ. The symbols are results obtained by a numerical solution of (36) and (37). The limit $L/(2\pi) \gg 1$ corresponds to the analytical solution computed in Appendix B.

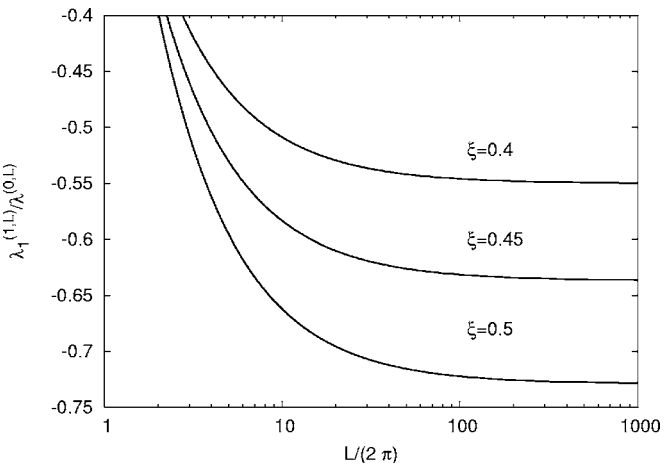

FIG. 5. Results for the quantity $\lambda_1^{(1,L)}/\lambda^{(0,L)}$ as a function of the dimensionless ratio $L/(2\pi)$ for various values of ξ.

$$F(\xi) = \xi\int_0^1 \frac{[1-\cos(s\pi\xi)](1-s^2)ds}{\cos(s\pi\xi)-\cos(\pi\xi)}. \tag{46}$$

A graph of this function is given in Fig. 3. Its asymptotic behaviors for ξ near 0 and 1 are given by

$$F(\xi) \simeq \frac{1}{3}\xi + \frac{\pi^2}{36}\xi^3 + \frac{\pi^4}{450}\xi^5 + \mathcal{O}(\xi^7), \quad \xi \to 0 \tag{47}$$

and

$$F(\xi) \simeq -\frac{8}{\pi^2}\log(1-\xi), \quad \xi \to 1. \tag{48}$$

The ratio of $\lambda_1^{(1,L)}$ to $\lambda^{(0,L)}$ is shown in Fig. 5 and the relative magnitude of the correction to the slip length increases with the channel depth.

The correction $\lambda_2^{(1,L)}$ due to the change in the cross section of the channel is shown in Fig. 6, in which the inset is the ratio $\lambda_2^{(1,L)}/\lambda^{(0,L)}$ similar to Fig. 5. It should be noted that

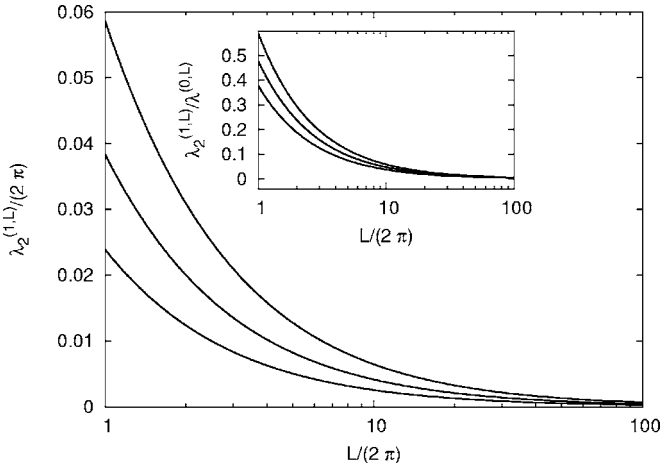

FIG. 6. Results for the quantity $\lambda_2^{(1,L)}/(2\pi)$ as a function of the dimensionless ratio $L/(2\pi)$ for various values of ξ: ξ=0.5 (top) ξ=0.45 (middle), and ξ=0.4 (bottom). Results are obtained by a numerical solution of (36) and (37). Inset: the ratio $\lambda_1^{(2,L)}/\lambda^{(0,L)}$ is also reported as a function of $L/(2\pi)$ for the same values of ξ as in the main figure.

this contribution to the slip length, as expected, has the same sign as ϵ and is, therefore, opposite to the previous one. This is an interesting point on which we comment in the next section.

VII. DISCUSSION AND CONCLUSIONS

Superhydrophobic surfaces are necessary to significantly affect pressure gradients and facilitate liquid flow in micrometer-scale channels. The superhydrophobic effect is realized by patterning the channel walls with posts or grooves so that the liquid forms a free surface and remains partially suspended away from the wall due to the effect of surface tension. While, on small scales, surface tension is a powerful force, it cannot prevent the free surface from deforming into or away from the gas, depending on the pressure difference $P^*_{\rm ch}-P^*_{\rm gas}$ between the liquid-filled channel and the gas. This circumstance has two effects: on the cross-sectional area of the flow passage and on the velocity field. As expected, the first effect increases or decreases the flow rate and, therefore, the slip length according to whether the liquid volume expands or contracts. The modification of the velocity field, on the other hand, reduces the slip length when the interface deforms. We have proven this conclusion analytically in the case of a deep channel, and numerically for finite depths. The physical origin of this phenomenon is due to the fact that, when the interface bows into the groove, the condition of free shear is moved below the level $y=0$ of the undisturbed surface so that, on $y=0$, there is a residual nonzero shear stress. The magnitude of the effect due to the change in the flow cross section relative to the modification of the velocity field decreases proportionally to the ratio of the pattern width to the channel height. For deep channels, the more significant effect is the second one, given in (45) and shown in Fig. 3. In principle, the opposite behavior of the two contributions to the effective slip length affords some degree of control on the flow rate by means of the magnitude and sign of $P^*_{\rm ch}-P^*_{\rm gas}$.

The magnitude of the effect that we have studied is quantified by the dimensionless ratio

$$\epsilon = \frac{H^*}{4\pi}\frac{P^*_{\rm ch}-P^*_{\rm gas}}{\sigma}. \tag{49}$$

The only existing data with which our theory can be compared are those reported by Ou and co-workers.[9] We can estimate from their Fig. 9 that the air-water interface protrudes 2–4 μm below the channel floor. The spatial period of the grooves on their lower wall is $H^*=60$ μm. Our parameter ϵ is therefore of the order of $(2-4)/60=0.03-0.06$, which produces only a very small correction to the unperturbed solution. However, for periodicity patterns $H^*\sim 10$ μm, with $P^*_{\rm ch}-P^*_{\rm gas}\sim 100$ kPa, $\sigma\sim 0.1$ N/m, we have $\epsilon\sim 0.1$, an estimate that would increase further with increasing area fraction ξ as shown in Fig. 3.

ACKNOWLEDGMENT

M.S. is grateful to STW (Nanoned Programme) for financial support.

APPENDIX A

In this appendix, we solve the zeroth-order problem for a channel of infinite depth. In this limit, the appropriate situation to consider is that of a linear shear flow over a periodic array of free-slip longitudinal strips. We write the velocity field as the sum of a linear shear flow plus a perturbation $(\tilde{w}^{(0,\infty)})$,

$$w^{(0,\infty)}(x,y) = y + \tilde{w}^{(0,\infty)}(x,y), \tag{A1}$$

with the correction expanded as

$$\tilde{w}^{(0,\infty)}(x,y) = \frac{a_0^{(0,\infty)}}{2} + \sum_{n=1}^{\infty} a_n^{(0,\infty)} \cos(nx) e^{-ny}. \tag{A2}$$

The boundary conditions (4) and (5) give rise to the dual series problem

$$\frac{a_0^{(0,\infty)}}{2} + \sum_{n=1}^{\infty} a_n^{(0,\infty)} \cos(nx) = 0, \quad c < x < \pi, \tag{A3}$$

$$\sum_{n=1}^{\infty} a_n^{(0,\infty)} n \cos(nx) = 1, \quad 0 < x < c. \tag{A4}$$

For the problem

$$\frac{1}{2}a_0^{(0,\infty)} + \sum_{n=1}^{\infty} a_n^{(0,\infty)} \cos(nx) = 0, \quad c < x < \pi, \tag{A5}$$

$$\sum_{n=1}^{\infty} n a_n^{(0,\infty)} \cos(nx) = f(x), \quad 0 < x < c, \tag{A6}$$

Sneddon (p. 161)[23] gives the solution

$$a_0^{(0,\infty)} = \frac{2}{\pi}\left[\frac{\pi}{\sqrt{2}}\int_0^c h_1^{(0,\infty)}(t)dt\right], \tag{A7}$$

$$a_n^{(0,\infty)} = \frac{2}{\pi}\left[\frac{\pi}{2\sqrt{2}}\int_0^c h_1^{(0,\infty)}(t)[P_n(\cos t) + P_{n-1}(\cos t)]dt\right], \quad n = 1,2,\ldots, \tag{A8}$$

with P_n Legendre polynomials. The function $h_1^{(0,\infty)}(t)$ is

$$h_1^{(0,\infty)}(t) = \frac{2}{\pi}\frac{d}{dt}\int_0^t \frac{\sin\frac{x}{2}dx}{\sqrt{\cos x - \cos t}}\int_0^x f(u)du \tag{A9}$$

or, in our case,

$$h_1^{(0,\infty)}(t) = \frac{2}{\pi}\frac{d}{dt}\int_0^t \frac{x\sin\frac{x}{2}dx}{\sqrt{\cos x - \cos t}}. \tag{A10}$$

The computation of $a_0^{(0,\infty)}$ and of $\tilde{w}^{(0,\infty)}$ hinges on the knowledge of the function $h_1^{(0,\infty)}(t)$, which is the derivative of

$$I^{(0,\infty)}(t) = \frac{2}{\pi}\int_0^t \frac{x \sin\frac{x}{2} dx}{\sqrt{\cos x - \cos t}}. \tag{A11}$$

This integral can be evaluated with some manipulations and the use of formula 3.842 of Gradshteyn and Ryzhik[22] with the result

$$I^{(0,\infty)}(t) = 2\sqrt{2}\log\left(\frac{1}{\cos\frac{t}{2}}\right), \tag{A12}$$

from which

$$h_1^{(0,\infty)}(t) = \sqrt{2}\tan\frac{t}{2} \tag{A13}$$

and

$$\frac{a_0^{(0,\infty)}}{2} = 2\log\left(\frac{1}{\cos\frac{c}{2}}\right). \tag{A14}$$

We also notice that, from Sneddon (p. 161),[23]

$$\frac{1}{2}a_0^{(0,\infty)} + \sum_{n=1}^{\infty} a_n^{(0,\infty)}\cos(nx) = \cos\left(\frac{x}{2}\right)\int_x^c \frac{h_1^{(0,\infty)}(t)dt}{\sqrt{\cos x - \cos t}}, \tag{A15}$$

which immediately leads to the velocity at $y=0$,

$$\tilde{w}^{(0,\infty)}(x,0) = \sqrt{2}\cos\left(\frac{x}{2}\right)\int_x^c \frac{\tan\frac{t}{2}}{\sqrt{\cos x - \cos t}}dt, \quad |x| < c. \tag{A16}$$

This integral can be evaluated exactly leading to (31). The quantity $\partial_x \tilde{w}^{(0,\infty)}(x,0)$ is also readily evaluated with the result given in (33).

APPENDIX B

In this appendix, we solve the for first-order correction to the linear shear flow problem considered in Appendix A. We write the velocity correction as

$$w^{(1,\infty)}(x,y) = \frac{a_0^{(1,\infty)}}{2} + \sum_{n=1}^{\infty} a_n^{(1,\infty)}\cos(nx)e^{-ny} \tag{B1}$$

with the boundary conditions (4) for $c<x<\pi$ and

$$\partial_y w^{(1,\infty)}(x,0) = -\partial_x[\eta(x)\partial_x w^{(0,\infty)}(x,0)] \quad \text{for } 0<x<c.$$

Formulas (A7) and (A8) of Appendix A again apply with the function h_1 now given by

$$h_1^{(1,\infty)}(t) = \frac{2}{\pi}\frac{d}{dt}\int_0^t \frac{\sin\frac{x}{2}\eta(x)\partial_x w^{(0,\infty)}(x,0)dx}{\sqrt{\cos x - \cos t}} \tag{B2}$$

from which we have

$$a_0^{(1,\infty)} = \frac{2\sqrt{2}}{\pi}\int_0^c \frac{\sin\frac{x}{2}\eta(x)\partial_x w^{(0,\infty)}(x,0)dx}{\sqrt{\cos x - \cos c}} \tag{B3}$$

or, upon using (33) for $\partial_x w^{(0,\infty)}(x,0)$,

$$a_0^{(1,\infty)} = -\frac{4}{\pi}\int_0^c \frac{\sin^2\frac{x}{2}(c^2-x^2)dx}{\cos x - \cos c} = -\frac{2}{\pi}\int_0^c \frac{(1-\cos x)(c^2-x^2)dx}{\cos x - \cos c}. \tag{B4}$$

If we introduce the slip length as $\lambda_1^{(1,\infty)} = a_0^{(1,\infty)}/2$, when we express $\epsilon\lambda_1^{(1,\infty)}$ normalized to the pattern dimension, we obtain

$$\epsilon\frac{\lambda_1^{(1,\infty)}}{2\pi} = -\frac{1}{4\pi^2 R}\int_0^c \frac{(1-\cos x)(c^2-x^2)dx}{\cos x - \cos c}. \tag{B5}$$

With $s=x/c$, $\delta=c^2/2R$, and $c=\pi\xi$, the previous expression becomes

$$\epsilon\frac{\lambda_1^{(1,\infty)}}{2\pi} = -\frac{\delta}{2\pi}F(\xi) \tag{B6}$$

in which

$$F(\xi) = \xi\int_0^1 \frac{[1-\cos(s\pi\xi)](1-s^2)ds}{\cos(s\pi\xi) - \cos(\pi\xi)}. \tag{B7}$$

A partial evaluation gives

$$F(\xi) = \frac{2}{\pi^3\xi^2}\tan\left(\frac{1}{2}\pi\xi\right)\left[\int_0^{2\pi\xi} S_1(\alpha)d\alpha - \pi\xi S_1(2\pi\xi)\right] - \frac{2}{3}\xi \tag{B8}$$

in which

$$S_1(\alpha) = \sum_{n=1}^{\infty}\frac{\sin(n\alpha)}{n^2} = \frac{1}{2}\int_0^{\alpha}\log\frac{1}{2(1-\cos y)}dy. \tag{B9}$$

Integration by parts leads to

$$S_1(\alpha) = \alpha\left[\log\frac{1}{2} - \log\sin\left(\frac{1}{2}\alpha\right)\right] + 2\int_0^{\alpha/2} x\cot x dx, \tag{B10}$$

where the last integral cannot be evaluated in closed form. The asymptotic results mentioned at the end of Sec. VI are readily derived from these expressions.

APPENDIX C

In this appendix, we briefly sketch the procedure used to solve the dual series equations numerically. We start from the general structure

$$\frac{A_0}{2} + \sum_{n=1}^{\infty}\Gamma_n A_n\cos(nx) = 0, \quad c<x<\pi, \tag{C1}$$

$$\sum_{n=1}^{\infty} n\Psi_n A_n \cos(nx) = f(x), \quad 0 < x < c \tag{C2}$$

with Γ_n and Ψ_n generic functions of n. The two expressions are multiplied by $\cos(mx)$ and integrated in their respective domains of validity. Upon using the identity

$$\int_0^c \cos(mx)\cos(nx)dx = \frac{\pi}{2}\delta_{nm} - \int_c^{\pi} \cos(mx)\cos(nx)dx, \tag{C3}$$

the result may be written as

$$\int_c^{\pi} \frac{A_0}{2}\cos(mx)dx + \sum_{n=1}^{\infty} \Gamma_n A_n \left(- \int_0^c \cos(mx)\cos(nx)dx + \frac{\pi}{2}\delta_{nm} \right) = 0, \tag{C4}$$

$$\sum_{n=1}^{\infty} n\Psi_n A_n \int_0^c \cos(nx)\cos(mx)dx = \int_0^c \cos(mx)f(x)dx. \tag{C5}$$

Upon adding these two relations, the result may be written in the form of a linear system,

$$\sum_{n=0}^{\infty} M_{n,m} A_n = B_m, \tag{C6}$$

where

$$M_{0,m} = \frac{1}{2}\int_c^{\pi} \cos(mx)dx, \tag{C7}$$

$$M_{n,m} = (n\Psi_n - \Gamma_n)\int_0^c \cos(mx)\cos(nx)dx + \frac{\pi}{2}\delta_{nm}\Gamma_n, \quad (n > 1), \tag{C8}$$

$$B_m = \int_0^c \cos(mx)f(x)dx. \tag{C9}$$

For the numerical evaluation, the linear system (C6) is truncated and reduced to a $N \times N$ matrix and the solution is then found to converge upon truncation refinement.

[1] E. Lauga, M. Brenner, and H. Stone, "Microfluidics: The no slip boundary condition," in *Handbook of Experimental Fluid Mechanics* (Springer, New York, 2007).
[2] J. T. Cheng and N. Giordano, "Fluid flows through nanometer-scale channels," Phys. Rev. E **65**, 031206 (2002).
[3] Y. Zhu and S. Granick, "Limits of the hydrodynamic no-slip boundary condition," Phys. Rev. Lett. **88**, 106102 (2002).
[4] J.-L. Barrat and L. Bocquet, "Large slip effect at a non-wetting fluid-solid interface," Phys. Rev. Lett. **82**, 4671 (1999).
[5] C. Cottin-Bizonne, C. Barentine, E. Charlaix, E. Bocquet, and J.-L. Barrat, "Dynamics of simple liquids at heterogeneous surfaces: Molecular dynamics simulations and hydrodynamic description," Eur. Phys. J. E **15**, 427 (2004).
[6] M. Sbragaglia, R. Benzi, L. Biferale, S. Succi, and F. Toschi, "Surface roughness-hydrophobicity coupling in microchannel and nanochannel flows," Phys. Rev. Lett. **97**, 204503 (2006).
[7] C.-M. Ho and Y.-C. Tai, "Micro-electro-mechanical systems (MEMS) and fluid flows," Annu. Rev. Fluid Mech. **30**, 579 (1998).
[8] P. Tabeling, *Introduction a la Microfluidique* (Belin, Paris, 2003).
[9] J. Ou, B. Perot, and J. Rothstein, "Laminar drag reduction in microchannels using ultra-hydrophobic surfaces," Phys. Fluids **16**, 4635 (2004).
[10] J. Ou and J. Rothstein, "Direct velocity measurements of the flow past drag-reducing ultra-hydrophobic surfaces," Phys. Fluids **17**, 103606 (2005).
[11] P. Joseph, C. Cottin-Bizonne, J.-M. Benoit, C. Ybert, C. Journet, P. Tabeling, and L. Bocquet, "Slippage of water past superhydrophobic carbon nanotube forests in microchannels," Phys. Rev. Lett. **97**, 156104 (2006).
[12] J. Bico, C. Marzolin, and D. Quere, "Pearl drops," Europhys. Lett. **47**, 220 (1999).
[13] D. Oner and T. J. McCarthy, "Ultra-hydrophobic surfaces: Effects of topography length scale on wettability," Langmuir **16**, 7777 (2000).
[14] K. Watanabe, Y. Udagawa, and H. Udagawa, "Drag reduction of Newtonian fluid in a circular pipe with a highly repellent wall," J. Fluid Mech. **381**, 225 (1999).
[15] C.-H. Choi and C.-J. Kim, "Large slip of aqueous liquid flow over a nanoengineered superhydrophobic surface," Phys. Rev. Lett. **96**, 066001 (2006).
[16] R. Benzi, L. Biferale, M. Sbragaglia, S. Succi, and F. Toschi, "Mesoscopic modelling of heterogeneous boundary conditions for microchannel flows," J. Fluid Mech. **548**, 257 (2006).
[17] E. Lauga and H. Stone, "Effective slip length in pressure driven Stokes flow," J. Fluid Mech. **489**, 55 (2003).
[18] J. Philip, "Flow satisfying mixed no-slip and no-shear conditions," Z. Angew. Math. Phys. **23**, 353 (1972).
[19] M. Sbragaglia and A. Prosperetti, "Effective velocity boundary condition at a mixed slip surface," J. Fluid Mech. **578**, 435 (2007).
[20] N. V. Priezjev, A. A. Darhuber, and S. M. Troian, "Slip behavior in liquid films on surfaces of patterned wettability: Comparison between continuum and molecular dynamics simulations," Phys. Rev. E **71**, 041608 (2005).
[21] J. Davies, D. Maynes, B. W. Webb, and B. Woolford, "Laminar flow in a microchannel with superhydrophobic walls exhibiting transverse ribs," Phys. Fluids **18**, 087110 (2006).
[22] I. S. Gradshteyn and I. M. Ryzhik, *Table of Integrals, Series, and Products*, 6th ed. (Academic, San Diego, 2000).
[23] I. N. Sneddon, *Mixed Boundary Value Problems in Potential Theory* (North-Holland, Amsterdam, 1966).